Differential gene expression and gene variants drive color and pattern development in divergent color morphs of a mimetic poison frog

Adam M M Stuckert*[1,2], Tyler Linderoth[3], Matthew D MacManes[2], Kyle Summers[1]

[1]Department of Biology, East Carolina University

[2]Department of Molecular, Cellular & Biomedical Sciences, University of New Hampshire

[3]Department of Integrative Biology, University of California Berkeley

*corresponding author: adam.stuckert@unh.edu

Abstract:

Evolutionary biologists have long investigated the ecological contexts, evolutionary forces, and proximate mechanisms that produce the diversity of animal coloration we see in the natural world. In aposematic species, color and pattern is directly tied to survival and thus understanding the origin of the phenotype has been a focus of both theoretical and empirical inquiry. In order to better understand this diversity, we examined gene expression in skin tissue during development in four different color morphs of the aposematic mimic poison frog, *Ranitomeya imitator*. We identified a suite of candidate color-related genes *a priori* and identified the pattern of expression in these genes over time, differences in expression of these genes between the mimetic morphs, and genetic variants that differ between color morphs. We identified several candidate color genes that are differentially expressed over time or across populations, as well as a number of color genes with fixed genetic variants between color morphs. Many of the color genes we discovered in our dataset are involved in the canonical Wnt signaling pathway, including several fixed SNPs between color morphs. Further, many genes in this pathway were differentially expressed at different points in development (e.g., *lef1, tyr, tyrp1*). Importantly, Wnt signaling pathway genes are overrepresented relative to expression in *Xenopus tropicalis.* Taken together, this provides evidence that the Wnt signaling pathway is contributing to color pattern production in *R. imitator,* and is an excellent candidate for producing some of the differences in

color pattern between morphs. In addition, we found evidence that sepiapterin reductase is likely important in the production of yellow-green coloration in this adaptive radiation. Finally, two iridophore genes (*arfap1, gart*) draw a strong parallel to previous work in another dendrobatid, indicating that these genes are also strong candidates for differential color production. We have used high throughput sequencing throughout development to examine the evolution of coloration in a rapid mimetic adaptive radiation and found that these divergent color patterns are likely to be affected by a combination of developmental patterns of gene expression, color morph-specific gene expression, and color morph-specific gene variants.

Introduction:

The diversity of animal coloration in the natural world has long been a focus of investigation in evolutionary biology. Color phenotypes are profoundly impacted by both natural and sexual selection, and color phenotypes are often under selection from multiple biotic and abiotic factors (Rudh and Qvarnström 2013). For example, in some species color pattern has evolved in the context of both predator avoidance and thermoregulation (Hegna et al. 2013). The underlying mechanisms behind color and pattern phenotypes are of general interest, particularly in systems in which color phenotypes are variable and yet likely to be under intense selection.

One such example are adaptive radiations, in which selection produces rapid phenotypic diversification within a species or group of species. Well-documented examples of adaptive radiations that involve variation in coloration include sticklebacks (Schluter 1995), cichlid fishes (Seehausen 2006), and Hawaiian spiders (Gillespie 2004). Adaptive radiations can be driven by various factors, including strong, frequency dependent selection imposed by predation (Nosil and Crespi 2006). The dendrobatid mimic poison frog (*Ranitomeya imitator*) underwent a rapid adaptive radiation to mimic established

49 congenerics (*R. fantastica, R. summersi,* and *R. variabilis*) in order to gain protection from predators—a
50 case of Müllerian mimicry (Symula et al. 2001, 2003; Stuckert et al. 2014b,a). For these frogs and other
51 Müllerian mimics, it is clear that the comimetic species experience strong selection to maintain local
52 color phenotypes (e.g. *Heliconius* butterflies (Mallet and Barton 1989), velvet ants (Wilson et al. 2015),
53 and millipedes (Marek and Bond 2009)). Although evolutionary theory has historically predicted that
54 mimicry (and aposematism in general) should be locally monomorphic, geographic variation in color and
55 pattern appear to be the norm in both aposematic and mimetic species (Joron and Mallet 1998; Briolat
56 et al. 2018).

57 This kind of variation has long been a focus of scientific interest at both the proximate and
58 ultimate level. Several experiments have revealed that local predators exert purifying selection on
59 aposematic phenotypes (Hensel and Brodie 1976; Hegna et al. 2011; Paluh et al. 2014). However, over
60 geographic distances heterogeneity in local predator communities and genetic drift in aposematic
61 species are likely sufficient to produce the geographical mosaics in color and pattern seen in many
62 aposematic and mimetic species (Ruxton et al. 2004; Sherratt 2006; Nokelainen et al. 2012).
63 Determining the underlying genetic architecture of these changes has been a primary thrust of research
64 in recent decades, because this allows researchers to examine both selection on these genes and
65 associated phenotypes as well as convergence at the molecular level within and between parallel
66 adaptive radiations.

67 Researchers have been able to pin down some key genetic loci in *Heliconius* butterfly mimicry
68 systems (e.g., *WntA* (Martin et al. 2012) and *optix* (Reed et al. 2011; Supple et al. 2013)), though there
69 are many others likely involved as well (Kronforst and Papa 2015). Interestingly, it seems that only a
70 handful of loci control the different phenotypes in certain mimetic complexes, and that supergenes may
71 be critically important in the diversity of mimetic phenotypes seen in *Heliconius* Müllerian mimicry
72 systems and *Papilio* Batesian mimicry systems (Kunte et al. 2014; Kronforst and Papa 2015; Nishikawa et

al. 2015). While the generality of this trend remains unclear, preliminary evidence from an analogous mimetic radiation of poison frogs indicates that this pattern may be found in this system as well (Vestergaard et al. 2015).

Amphibian coloration is linked to three structural chromatophore types (melanophores, iridophores, and xanthophores) and the pigments deposited in them (Mills & Patterson 2009). Dark coloration is produced by melanophores and the melanin pigments found inside them, including blacks, browns, and dark greens (Duellman and Trueb 1986). While the melanophores contribute to how dark a green color is, greens and blues are largely structurally produced, with hue mainly determined by the reflection of light from iridophores (Bagnara et al. 2007), which depends on the presence and orientation of guanine platelets, where thicker platelets tend to reflect longer wavelengths of light (Ziegler 2003; Bagnara et al. 2007; Saenko et al. 2013). Yellow, orange and red coloration are dependent on pigments such as pteridines and carotenoids that absorb different wavelengths of light, and are deposited within xanthophores (Duellman and Trueb 1986).

Here we characterize the genetic architecture of coloration in this adaptive radiation by examining gene expression and its timing across a developmental time series of the skin of the Peruvian mimic poison frog. This poison frog has evolved to converge on the appearance of sympatric congeners and is therefore polytypic with substantial geographic variation in the color phenotype (Symula et al. 2001, 2003). Thus, this species provides a good opportunity to examine gene expression as it relates to color and pattern in an adaptive radiation. Color in this species begins to appear early during development while individuals are still tadpoles, which is consistent with observations that chromatophores develop from the neural crest early in embryonic development (DuShane 1935). We examined gene expression patterns using RNA sequencing from four different mimetic color populations of *R. imitator* (Figure 1), each at four different time points during development. These different color morphs represent a variety of both colors and patterns, providing an opportunity to examine the

97 underlying genetic basis of these traits. First, we consider overall gene expression patterns during
98 development and across color morphs. Then we examine expression, timing, and morph-based
99 differences of candidate color genes compiled from previous research on other taxa. This approach
100 allows us to carefully examine the genomics underlying mimicry in poison frogs. Further, our approach
101 provides insight into the genetic architecture of color and pattern in amphibians, which has historically
102 been a challenge due to their large genomes. We discuss our findings in the context of what is known
103 about color production in amphibians as well as the adaptive radiation that produced these color
104 phenotypes.

105

106 **Methods:**

107 *Tadpole collection:*

108 The initial breeding stock of *Ranitomeya imitator* was purchased from Understory Enterprises,
109 LLC (Chatham, Canada). Frogs used in this project represent captive-bred individuals sourced from the
110 following wild populations: Baja Huallaga (yellow-striped morph), Sauce (orange-banded), Tarapoto
111 (green-spotted), and Varadero (redheaded; see Figure 1). Breeding *R. imitator* pairs were placed in 5-
112 gallon terraria containing small (approximately 13 cm) PVC pipes capped on one end and filled halfway
113 with water. We removed tadpoles from the tanks after the male transported them into the pools of
114 water and hand reared them. Although in the wild female *R. imitator* feed their tadpoles unfertilized
115 eggs, tadpoles can survive and thrive on other food items (Brown et al. 2008). We raised experimental
116 tadpoles on a diet of Omega One Marine Flakes fish food mixed with Freeze Dried Argent Cyclop-Eeze,
117 which they received three times a week, with full water changes twice a week until sacrificed for
118 analyses at 2, 4, 7, and 8 weeks of age. At two weeks, tadpoles are limbless, patternless, and a light gray
119 color with two dark black eyeballs. At 4 weeks tadpoles are a slightly darker gray and have back limb

buds. Tadpoles had developed their pattern and some coloration as well as reached the onset of metamorphosis at around week 7, and had metamorphosed, were resorbing the tail, and had their froglet patterns at 8 weeks old. Pattern development continues as juveniles and subadults frogs as they grow into the ultimate pattern they possess as adults. Our four sampling periods correspond to roughly Gosner stages 25, 27, 42, and 44 (Gosner 1960). We sequenced a minimum of three individuals at each time point from the Sauce, Tarapoto, and Varadero populations (except for Tarapoto at 8 weeks), and two individuals per time point from the Huallaga population. Individuals within the same time points were sampled from different family groups (Table 1).

Figure 1. Representatives of the four color morphs of *Ranitomeya imitator* used in this study. Clockwise from top left: orange-banded morph from Sauce, yellow-striped morph from Baja Huallaga, redheaded morph from Varadero, and the green-spotted morph from Tarapoto.

Tadpoles were anesthetized with 20% benzocaine (Orajel), then sacrificed via pithing. The entirety of the skin was removed and stored in RNA later (Ambion) at -20° C until RNA extraction. RNA was extracted from the whole skin using a standardized Trizol protocol, cleaned with DNAse and RNAsin, and purified using a Qiagen RNEasy mini kit. Libraries were prepared using standard poly-A tail purification with Illumina primers, and individually barcoded using a New England Biolabs Ultra Directional kit as per the manufacturer's protocol. Individually barcoded samples were pooled and sequenced using 50 bp paired end reads on three lanes of the Illumina HiSeq 2500 at the New York Genome Center. This yielded on average 24.45M reads per library ± 8.6M sd (range: 10.1-64.M).

Transcriptome assembly:

Choosing a single individual or treatment to assemble a transcriptome could plausibly influence the quality of our transcriptome and bias our results. Therefore, in order to generate a reference transcriptome we assembled 40 M randomly subsampled forward and reverse reads sampled across morphs and time points using seqtk (https://github.com/lh3/seqtk) and used the Oyster River Protocol version 1.1.1 (MacManes 2017) to assemble this dataset. Evidence indicates that there is a substantial diminishment of returns in terms of transcriptome assembly completeness from using over 20-30 million reads (MacManes 2017). Initial error correction was done using RCorrector 1.01, followed by adaptor removal and quality trimming using trimmomatic version 0.36 at a Phred score of ≤ 3 (Bolger et al. 2014) since over-rigorous quality trimming has been shown to reduce assembly completeness (MacManes 2014). The Oyster River Protocol (MacManes 2017) assembles a transcriptome by merging multiple assemblies constructed using a series of different transcriptome assemblers and kmer lengths. We constructed the Independent assemblies with Trinity version 2.4.0 (Grabherr et al. 2011), Shannon version 0.0.2 (Kannan et al. 2016), and SPAdes assembler version 3.11 using 35-mers (Bankevich et al. 2012). This deviates slightly from the Oyster River Protocol specified in MacManes (2017), which

158 specifies kmer lengths of 55 and 75 for SPAdes assemblies, but that exceeds our 50 bp sequencing read
159 length. We then merged these individual assemblies using OrthoFuser (MacManes 2017). Finally, we
160 assessed transcriptome quality using BUSCO version 3.0.1 (Simão et al. 2015) and TransRate 1.0.3
161 (Smith-Unna et al. 2016).

162

163 *Downstream analyses:*

164 We used Diamond version 0.9.10 (Buchfink et al. 2015) to annotate our transcriptome with the
165 peptide databases for *Xenopus tropicalis*. We then pseudo-quantified alignments for each library and
166 technical replicate using Kallisto version 0.43.0 (Bray et al. 2016) and tested for differential gene
167 expression in R version 3.4.2 (R Core Team 2017) using Sleuth version 0.29.0 (Pimentel et al. 2017). We
168 accounted for the fact that samples were sequenced on three separate lanes by treating the lane that
169 each sample was sequenced on as a fixed effect in our linear models. We tested for a significant change
170 in gene expression driven by tadpole age with a likelihood ratio test. The alternative model involving
171 tadpole age was fit with the sequencing lane on which libraries were sequenced as fixed effects using
172 the R 'splines' library. Similarly, the null model that excluded tadpole age was fit with sequencing lane
173 treated as a fixed effect. We also tested for differential gene expression between color morphs using
174 likelihood ratio tests, correcting for multiple comparisons with a Benjamini-Hochberg-adjusted False
175 Discovery Rate and using a significance threshold of $\alpha = 0.05$. Specifically, for each gene we compared a
176 model involving color morph to one without color morph while controlling for batch effects by treating
177 sequencing lane as a fixed effect. In addition to examining overall differential expression, we examined
178 differential expression in an *a priori* group of candidate color genes which we collated from the
179 literature on other taxa (see code repository). We also used PANTHER version 14.0 (Mi et al. 2017) to
180 determine if any pigmentation or color gene pathways were statistically overrepresented in our dataset.

We conducted two separate overrepresentation tests, one with the genes differentially expressed over time and a second with the genes differentially expressed between color morphs. Tests were conducted using *Xenopus tropicalis* as a reference, and a Fisher's exact test with a Benjamini–Hochberg False Discovery Rate correction for multiple comparisons. Finally, we generated hypotheses about candidate genes by examining SNPs that were fixed between color morphs. To do this we used ANGSD to identify SNPs showing fixed differences between morphs (Korneliussen et al. 2014). For SNP calling we only retained reads with a minimum base quality score of 20, sites with a minimum depth of 100 reads and at least six individuals, and used a p value threshold of 0.000001. Following SNP calling, we examined SNPS that were fixed in at least one color morph and were in our candidate color gene list. We then used BLAST translated nucleotide to protein searches (tblastx) to align the color morph specific gene variants to the best amino acid sequence match in the model species genome (either *Xenopus* or *Nanorana*). We confirmed codon frame by aligning the specific protein sequence from the model species (*Xenopus* or *Nanorana*) to the matching translated nucleotide sequence for each candidate gene in *R. imitator*. We then determined whether the color morph specific fixed variants produced synonymous or non-synonymous changes or introduced stop codons.

Color Morph	Time point (weeks)	N
Huallaga	2	2
Huallaga	4	2
Huallaga	7	2
Huallaga	8	2
Sauce	2	3
Sauce	4	3
Sauce	7	3
Sauce	8	3

Tarapoto	2	4
Tarapoto	4	4
Tarapoto	7	4
Tarapoto	8	1
Varadero	2	3
Varadero	4	3
Varadero	7	3
Varadero	8	3

198

199 Table 1. Sample sizes by color morph and tadpole age.

200 **Results:**

201 *Data and code availability:*

202 All read data are archived with the European Nucleotide Archive (accession number PRJEB28312). Code
203 for transcriptome assembly, annotation, and downstream analyses are all available on GitHub
204 (https://github.com/AdamStuckert/Ranitomeya-imitator-Developmental-Series). Our candidate color
205 genes are available in the same GitHub repository, and for the purposes of review, our assembled
206 transcriptome is publicly available in our GitHub repository.

207

208 *Transcriptome assembly:*

209 The Oyster River Protocol (MacManes 2017), produced a a transcriptome assembly that contained
210 88,182 total transcripts. When we ran BUSCO against the eukaryote database, our BUSCO score was
211 93.1% ([S:74.9%,D:18.2%],F:5.6%,M:1.3%,n:303), indicating that our transcriptome contained the
212 majority of conserved genes that we would expect to see in a eukaryotes. The transrate score for the
213 assembly, which measures contig accuracy, completeness, and non-redundancy, was 0.32505. Transrate
214 scores in the 0.2-0.3 range are considered good, and scores above 0.3 are considered very good (Smith-
215 Unna et al. 2016). We pseudoaligned reads from each library to our reference transcriptome with a

mapping rate of 88.2% ± 1.1% SD. Using *Xenopus tropicalis (NCBI Resource Coordinators 2016)* as our annotation database we successfully annotated 35,014 transcripts (39.7% of our total transcriptome), which corresponds to roughly 10,300 unique genes.

Differential expression and gene variants:

We found a total of 3,619 genes differentially expressed between time points in development. Among these genes, 111 of them were in our *a priori* color gene list of 501 genes (color gene list collated in the code repository). We also found 837 genes that were differentially expressed between color morphs of *Ranitomeya imitator.* Of these, we found 15 genes (Figure 2) in our *a priori* color gene list. Three genes (*recql4, sema3c,* and *tspan36*) were differentially expressed over time and between color morph.

GENE	TIME	COLOR MORPHS	NUMBER OF SNPS
adam17	X		
adh1		X	
adsl	X		
ak1	X		1
aldh1a1	X		
ap3d1	X		5
apc	X		1
arcn1			1
arfgap1			1
arfgap2			1
atic			2
atp12a	X		1
atp6ap2			1
atp6v0d1	X		
atp6v1h	X		1
atp7b	X		
atrn	X		6
axin2	X		2
bbs1		X	2
bcl2	X		
bloc1s3		X	
bmpr1a	X		
bnc2	X		
casp3	X		1
chm			2
crabp2			1

creb1			1
csf1r	X		
ctr9			1
dct	X		
dock7	X		2
dph1	X		
dst			2
ebna1bp2	X		
edar	X		
ednrb2	X		3
egfr	X		3
elovl3			1
en1	X		
erbb3			1
fgfr2	X		
foxn1	X		1
gart			2
gas1	X		1
gata3	X		
gchfr		X	
ggt1	X		
gja5	X		
gmps			4
gna11	X		
gne	X		1
gpc3	X		
gpnmb	X		
gpr143	X		
hells			9
herc2	X		
hps3			1
hps4		X	
hps5	X		
hps6			2
impdh2	X		
inpp5b	X		1
itgb1			10
kcnj13	X		
kitlg	X		
krt17	X		
lef1	X		
lrat	X		
lyst	X		
map2k1	X		
mcoln3	X		
med1	X		
med12	X		
mib1	X		
mlph	X		
mpzl3	X		
mycbp2	X		
myo5a			1
nf1	X		

notch1	X		
notch2	X		
nsf	X		1
oca2	X		
ovol1	X		
pabpc1	X		
pah	X		
paics.1	X		
pax3	X		
pcbd1		X	1
pck2	X		
pdgfb	X		
pdpk1	X		
pgk1	X		
pgm2	X		
phactr4	X		
pmel	X		
pnp	X		
ppat			1
prtfdc1			1
psen1			1
qdpr	X		1
rab27a			2
rab27b	X		
rab32	X		
rab38	X		
rab5d	X		
rabggta		X	
rdh10	X		8
recql4	X	X	
retsat	X		2
ric8b			2
rlbp1	X		
rpl24	X		
rps19	X		
rps20	X		
s1pr2	X		
scarb2	X		
sema3c	X	X	
sema4a	X		2
sfxn1		X	
shmt2	X		2
shroom2	X		1
skiv2l2	X		1
sla	X		
slc24a4	X		
slc24a5	X		
slc31a1	X		
slc45a2	X		
snai2	X		
sox10	X		1
sox18	X		
sox9	X		

spr		X	
sulf1	X		
tfap2a	X		
timp3	X		
traf6		X	
trappc6a	X		
trim33	X		1
trpm1	X		1
tspan36	X	X	1
ttc8		X	1
tyr	X		
tyrp1	X		
vps11			1
vps18		X	
vps39	X		
vsx2			2
wnt3			4
xdh	X		1

Table 2. Statistically significant color genes in this study. Columns represent differentially expressed genes across time, differentially expressed genes across color morphs, and finally the number of fixed SNPs in that gene between color morphs. An "X" represents a gene is significant, numbers in the final column represent the number of fixed SNPs.

We identified a total of 194,445 SNPs on 6,507 genes. We found 115 SNPs among contigs annotated as potential color genes according to our a priori list that were fixed between color morphs; these represented 58 unique candidate color genes. Of these SNPs, 63 represented synonymous changes, while 52 represented non-synonymous changes (Supplemental Table 1). Overall, our results illuminate 150 candidate color genes that vary over time, between morphs, or have SNP differences between morphs.

We also looked for evidence of statistical overrepresentation in pathways that contribute to color and pattern production. When we examined overrepresentation across time, we found no enrichment of pathways related to iridophore or xanthophore production or function. We did, however, find

241 overrepresentation in the Wnt signaling pathway over developmental time. The canonical Wnt signaling
242 pathway exhibited 2.11-fold enrichment (GO category: 0060070, p value = 0.00139, FDR corrected p
243 value = 0.0184), the regulation of Wnt signaling pathway exhibited a 1.76-fold enrichment (GO category:
244 0030111, p = 0.00208, FDR corrected p value = 0.0259), the Wnt signaling pathway exhibited a 1.59-fold
245 enrichment (GO category: 0016055, p = 0.00112, FDR corrected p value = 0.0155), and cell-cell signaling
246 by Wnt exhibited a 1.59-fold enrichment (GO category: 0198738, , p = 0.00112, FDR corrected p value =
247 0.0155). Additionally, we found that the generic pigmentation pathway exhibited 2.02-fold enrichment
248 (GO category: 0043473, p = 0.000407, FDR corrected p value = 0.00653). When we examined
249 overrepresentation across color morphs, we found no overrepresented gene groups that were linked to
250 pigmentation. Results for overrepresentation over time and between color morphs can be found in
251 Supplemental Table 2 and 3 respectively.

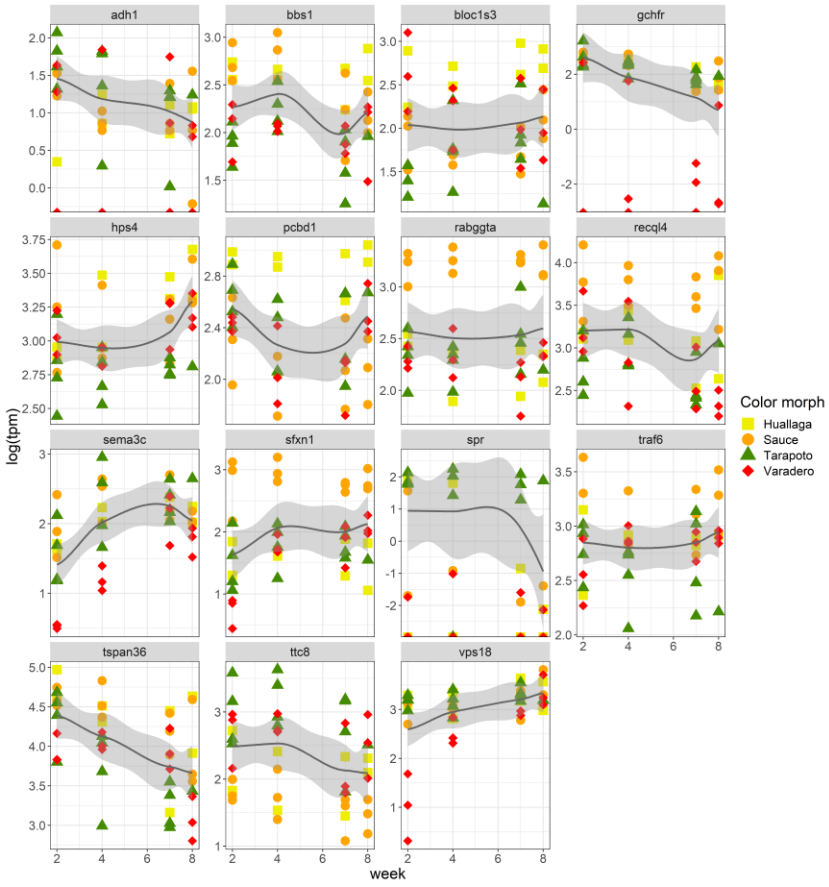

252

253 Figure 2. Expression patterns of genes which were differentially expressed between color morphs. Data
254 represented is the log of normalized transcripts per million from each individual. Trend line shows the
255 mean produced via loess smoothing across all samples and shaded gray areas represent 95% confidence
256 intervals.

257

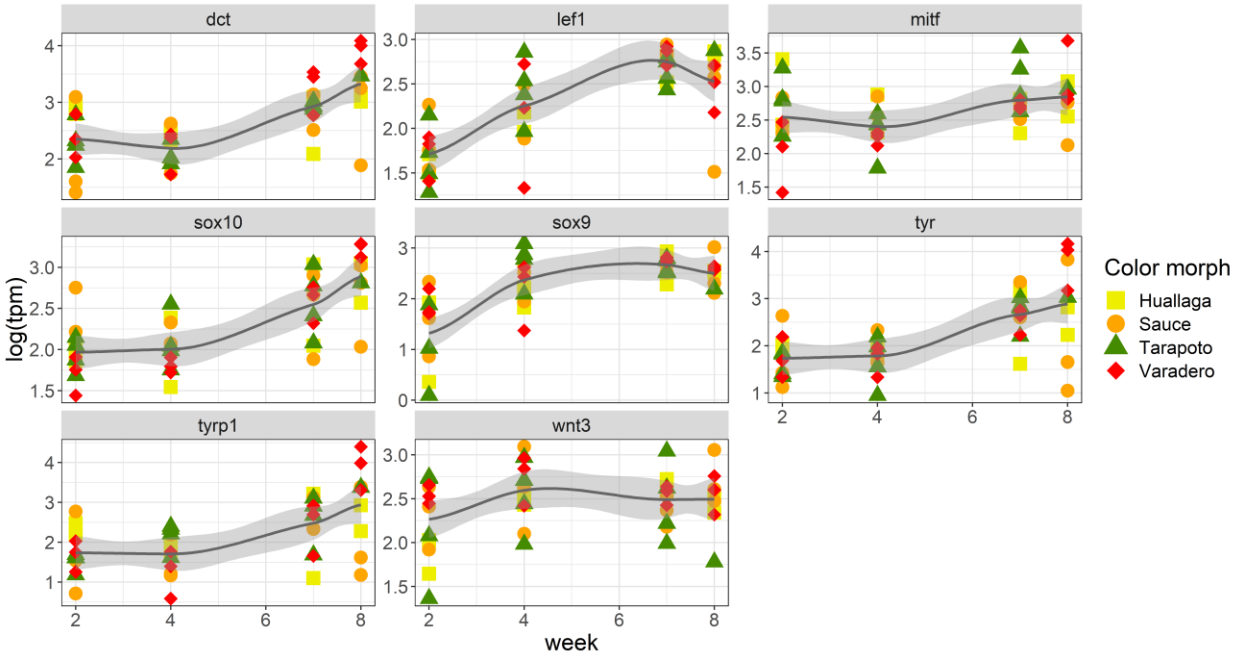

258

259 Figure 3. Expression patterns of selected genes in the *Wnt3* signaling pathway. Data represented is the
260 log of normalized transcripts per million from each individual. Trend line shows the mean produced via
261 loess smoothing across all samples and shaded gray areas represent 95% confidence intervals.

262

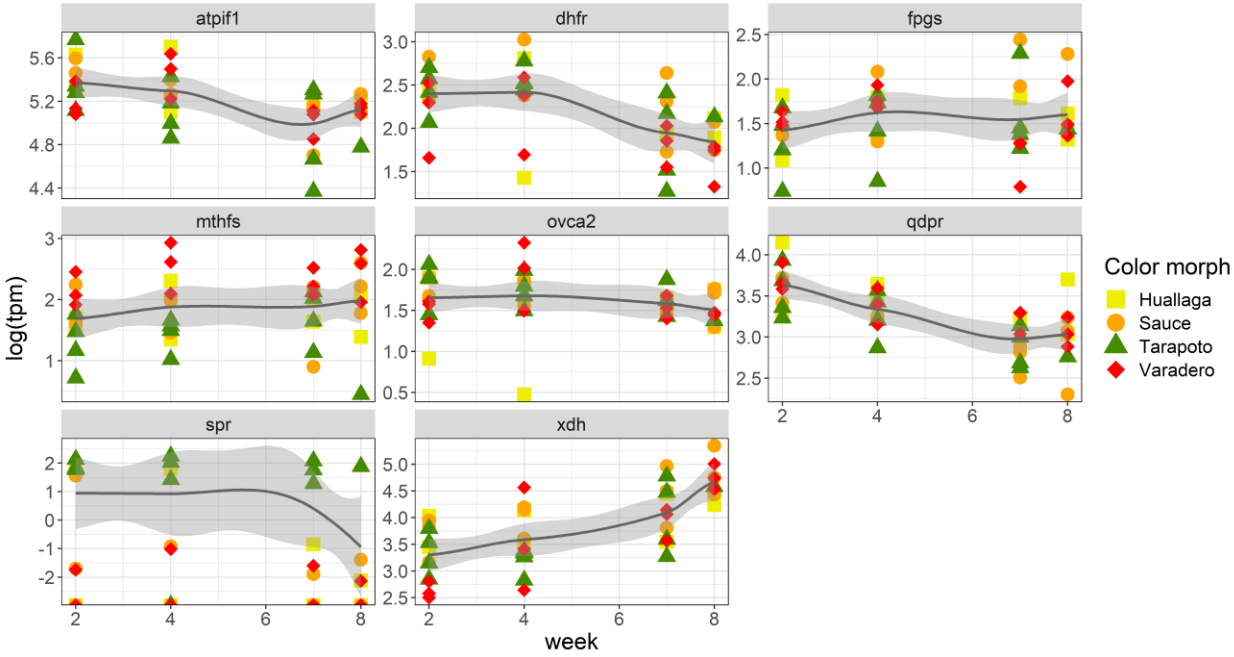

263

264 Figure 4. Expression patterns of selected pteridine genes. Data represented is the log of normalized

265 transcripts per million from each individual. Trend line shows the mean produced via loess smoothing

266 across all samples and shaded gray areas represent 95% confidence intervals.

267

268

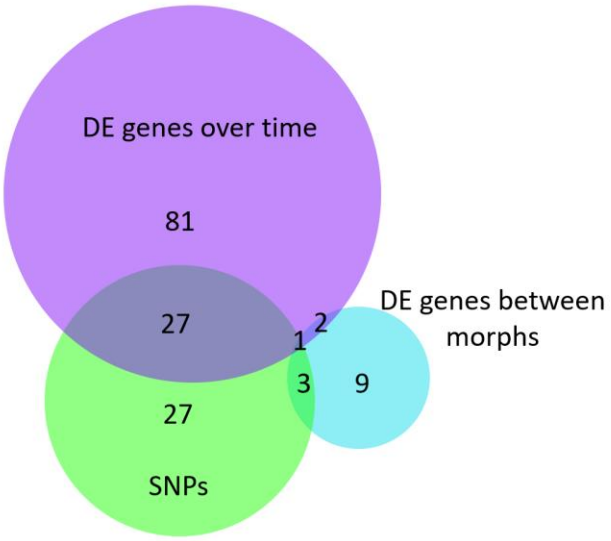

269

Figure 5. Venn diagram of genes differentially expressed over time (top left), differentially expressed between color morphs (right), and genes with fixed SNPs between color morphs (bottom).

Discussion:

The genetic, biochemical, cellular, physiological and morphological mechanisms that control coloration in adaptive radiations are of interest because of the obvious implications for survival and selection. Further, these mechanisms in amphibians are poorly characterized, particularly compared to better known groups like mammals and fish. Our results illuminate 150 candidate color genes that may be contributing to different color phenotypes between populations in a highly variable, polytypic poison frog. Specifically, we find differences in the developmental timing of gene expression (i.e., when these genes may be contributing to color and pattern formation) as well as differences in expression between different color morphs. Furthermore, we examined differences in coding region between morphs in order to generate hypotheses for sequence variants contributing to differentiation in color and pattern. We found fixed differences between color genes that are plausibly contributing to color and pattern differentiation between color morphs. Many of these are very promising candidates for controlling color and pattern, but the limited sample sizes in our study provide low power to accurately identify highly divergent sites and so this merits further sampling in future studies.

Wnt signaling pathway:

The canonical Wnt signaling pathway is important for the production of coloration, and Wnt genes have been shown to control differential color patterns in certain species (e.g., Kronforst et al. 2006; Martin et al. 2012; Gallant et al. 2014; Martin and Reed 2014). We found that several gene

ontology pathways involving the Wnt signaling pathways were overrepresented among genes showing differential expression over time (although not between color morphs), indicating that this is likely an important pathway for color production. Additionally, we found several genes in the Wnt signaling pathway with fixed allele differences. Perhaps the most intriguing of these is *wnt3* (Wingless-related integration site 3). *Wnt3 is a* gene with major effects on melanocyte-related coloration, as it is part of the canonical Wnt signaling pathway. This gene has been shown to upregulate many genes related to melanocyte production and melanin synthesis, including *mitf* (microphthalmia-associated transcription factor)*, tyr* (tyrosinase)*, tyrp1* (tyrosinase-like protein 1)*, lef1* (lymphoid enhancer binding factor 1)*,* and *sox10* (SRY-Box 10)(Takeda et al. 2000; Guo et al. 2012). We found four color morph specific SNPs in *wnt3*, two of which had non-synonymous changes. Although we did not find any color morph specific expression of *wnt3* or the aforementioned downstream targets, we did find that expression patterns of genes affected by *wnt3* (*lef1, tyr, tyrp1*) change throughout development, which is further corroborated by evidence that Wnt signaling pathway genes are overrepresented throughout development. Other genes with fixed SNPs that fall into the Wnt signaling pathway are *sox10, erbb3, axin2,* and *apc.* The presence of genomic variants fixed between color morphs in wnt3 and other Wnt signaling genes, significant changes in downstream targets throughout development, and the overrepresentation of these pathways in our dataset provides evidence that the Wnt signaling pathway is involved in pigment production and is putatively involved in the development of different color phenotypes in poison frogs. However, this requires validation, as Wnt and related genes are involved in early general development and therefore the overrepresentation of this pathway may or may not be a driving agent of color and pattern production/divergence in this species.

Wnt3 is capable of inhibiting *erbb3,* and this inhibition contributes to increased Wnt signaling (Jullien et al. 2012). Potentially, the SNP in *erbb3* is associated with similar effects on Wnt signaling. Additionally, beta-catenin is a key part of the Wnt signaling pathway. In the absence of Wnt signaling

316 beta-catenin is bound by a multiprotein complex involving *apc* (adenomatous polyposis coli), *axin* (axis
317 inhibition protein), and *gsk3beta* (glycogen synthase kinase 3 beta) which then degrades beta-catenin. In
318 fact, *apc* escorts beta-catenin to be degraded (Larue and Delmas 2006). However, this multiprotein
319 complex is dissociated when Wnt signaling occurs. Thus, the presence of fixed variants in *wnt3, apc,* and
320 *axin2* suggest that color variants in *Ranitomeya imitator* may be mechanistically controlled via the
321 maintenance of beta-catenin. Extracellular heparan sulfate proteoglycans which bind to Wnt ligands,
322 and modification of these by *sulf1* and *sulf2* (sulfatase 1 and sulfatase 2) can promote or reduce Wnt
323 signaling (Ai et al. 2003; Kleinschmit et al. 2010). We found a fixed SNP in the *sulf1* gene, which may also
324 be associated with the development of distinct color patterns. We acknowledge that SNP calling RNA-
325 seq data with our sample sizes does not indicate with certainty that these genes are contributing to
326 functional differences in phenotype between color morphs. However, we view these genes, especially
327 those within the Wnt signaling pathway, as particularly good candidates for future examination and
328 validation. More in-depth population level sampling could elucidate whether these genes are worth
329 pursuing functional validation.

330 The four morphs of *Ranitomeya imitator* used in this study have pattern elements on top of a
331 generally black dorsum and legs. In vertebrates, black coloration is caused by light absorption by
332 melanin in melanophores or (in mammals and birds) in the epidermis (Sköld et al. 2016). Melanophores
333 (and the other chromatophores) originate from populations of cells in the neural crest early in
334 development (Park et al. 2009). Given the timing of melanin synthesis and our sampling scheme, it is
335 logical that many of our differentially expressed candidate genes are in this pathway. Melanin is
336 synthesized from tyrosine, and this synthesis is influenced by a variety of different signaling pathways
337 (e.g., *Wnt*, *cAMP,* and *MAPK*), many of which influence *mitf* (known as the "master regulator gene" of
338 melanogenesis), a gene which encodes the melanogenesis associated transcription factor (Videira et al.
339 2013; D'Mello et al. 2016). It therefore makes sense that *mitf* is constitutively expressed across

340 populations and time in our study. The gene *creb1* (cAMP responsive element binding protein 1) is a
341 binding protein in the cAMP pathway, which ultimately influences the transcriptional factor *mitf,* and
342 the expression of this gene increases dramatically over time in *R. imitator* tadpoles as they show
343 increasing pigmentation. The upregulation of *creb1* causes *mitf* to increase melanin synthesis (D'Mello
344 et al. 2016). Intriguingly, frogs from the Varadero population typically have the lowest amount of black
345 overall (see Figure 1), and they also exhibit the lowest level of *mitf* expression. This, coupled with
346 evidence that *mitf* plays a role in the production of black versus brown coloration in the poison frog
347 *Dendrobates auratus (Stuckert et al. 2019)*, indicates that this gene likely plays a critical role in melanin
348 synthesis and the relative darkness of pigmentation in amphibians generally. This is logical, as *mitf* is
349 highly conserved throughout vertebrates (Lister et al. 1999).

350 The melanogenesis transcription factor increases melanin synthesis through an interaction with
351 the enzymes tyrosinase (*tyr*), tyrosinase-like protein 1 (*tyrp1*) and dopachrome tautomerase (*dct*), which
352 are key elements in melanin biosynthesis (Park et al. 2009). Although *tyr* is expressed even in our
353 youngest tadpoles, there is a dramatic increase in *tyr* expression over the course of development. During
354 this time, tadpoles go from a very light, almost transparent gray color to a much darker background
355 color with red, orange, yellow or green colored regions overlaying this black color. The phenotype and
356 correlated expression of *tyr* indicate that tyrosinase is likely a key component of melanin biosynthesis in
357 poison frogs. Similar to *tyr* expression, *tyrp1* expression substantially increased over time, a pattern
358 which is driven largely by high expression levels in the latest stages of the red-headed Varadero
359 tadpoles. Although we cannot say why this is with certainty, it may be because *tyrp1* seems to play a
360 role in switching melanin synthesis from the production of black eumelanin to more reddish
361 pheomelanin (note however that the evidence that *tyrp1* promotes this switch is controversial). Less
362 controversial however is that *tyrp1* has a strong influence on the ultimate color phenotype, particularly
363 in the presence of allelic variants in *tyrp1* (Rieder et al. 2001; Li et al. 2014). Further, upregulation of

364 *tyrp1* has been linked to the production of maroon rather than black plumage in quails and horses (Xu et
365 al. 2013; Li et al. 2014). Similarly, *tyrp1* is differentially expressed between color morphs of another
366 poison frog (Stuckert et al. 2019) in which frogs with lighter brown backgrounds have higher levels of
367 *tyrp1* expression than those of frogs with black backgrounds, providing some evidence that an increase
368 in expression of *tyrp1* may be related to the production of pheomelanin over eumelanin. However, this
369 is speculative, as to date pheomelanin has only been identified in one species of frog, *Pachymedusa*
370 *dacnicolor (Wolnicka-Glubisz et al. 2012)*. Given that *tyrp1* has been associated with pheomelanin and
371 red-brown colors, its expression in the redheaded Varadero population indicates that pheomelanin may
372 be contributing to red coloration in this population.

373 Similar to *tyrp1*, expression of *lef1* is associated with the production of pheomelanin, a pigment
374 associated with lighter color phenotypes (Song et al. 2017; Stuckert et al. 2019). We see early expression
375 of *lef1* which rapidly drops off until there is functionally no expression by the end of development when
376 melanic coloration becomes most obvious in tadpoles. The gene *sox9* (sex determining region Y – box 9)
377 also influences the transcription factor *mitf.* However, unlike *lef1* which leads to lighter pigmentation,
378 *sox9* is upregulated during melanocyte differentiation and can be activated by UVB exposure (Cheung
379 and Briscoe 2003). In our dataset, *sox9* is constitutively expressed across color morphs and times points,
380 but with a substantial decline in the later time points. Although tadpoles are still becoming darker, and
381 thus seem to be producing melanin at the late stages, the decrease in *sox9* expression in our dataset is
382 likely linked to a decrease in *mitf* activation and melanocyte differentiation. Further, *sox9* is expressed in
383 higher levels in darker color morphs of other frog species (Stuckert et al. 2019). This evidence indicates
384 that *sox9* may be an important determinant of color in amphibians generally, and poison frogs
385 specifically. Just as *sox9* is expressed most intensely in the populations with the most black skin, we see
386 the same pattern in *kit* (KIT proto-oncogene receptor tyrosine kinase), a membrane receptor that is
387 involved in one of the earliest steps of the melanogenesis pathway (D'Mello et al. 2016). Ultimately the

388 pathway involving *kit* influences the same transcription factor as *sox9* (*mitf*), so these may be
389 complementary genetic mechanisms that produce similar effects.

390 In addition to the interaction between fixed SNPs and gene expression of downstream targets,
391 *wnt3a* is of note because it has analogous effects on coloration in the *Heliconius* butterflies of Central
392 and South America. Both the frogs and the butterflies are classic Neotropical examples of aposematism.
393 Furthermore, our study species *Ranitomeya imitator* is also involved with Müllerian mimicry complexes
394 just as *Heliconius* butterflies are. It has repeatedly been established that *WntA* controls melanization in
395 the forewing in both *Heliconius* and *Limnetis* butterflies and delineates lighter-colored patches.
396 Furthermore, other Wnt genes (e.g., *wg, Wnt6, Wnt10*) play a role in wing pigment patterning in
397 butterflies (Kronforst et al. 2006; Martin et al. 2012; Gallant et al. 2014; Martin and Reed 2014). Our
398 data indicates that a Wnt gene is also a good candidate for producing differential colors and patterns in
399 poison frogs, and future work should aim to test this hypothesis. The possibility that organisms as
400 evolutionarily distant as poison frogs and butterflies show the same patterns of diversity, extremely
401 similar mimicry patterns, in the same exact geographic locations, with color phenotypes controlled by
402 differences in the same family of genes is intriguing.

403

404 *Iridophore genes:*

405 A number of candidate color genes related to iridophores showed sequence or expression
406 differences in our analyses. We found fixed, color morph specific SNPs in the gene *gart,* a gene which
407 catalyzes a number of steps in the *de novo* synthesis of purine (Ng et al. 2009). In zebrafish, mutations in
408 this gene show a drastic reduction in the overall number of iridophores and a much lighter phenotype
409 (Ng et al. 2009). Additionally, this gene has also been implicated in the differential production of green
410 and blue phenotypes in another poison frog (Stuckert et al. 2019). That same study also found that

411 *arfgap1* is differentially expressed between color morphs and likely contributes to differences in
412 iridophore-related coloration (Stuckert et al. 2019), and other work has indicated that *arfgap1* likely
413 contributes to guanine synthesis within iridophores in fish (Higdon et al. 2013). We found a fixed SNP
414 between color morphs in both *arfgap1* and *arfgap2* within our dataset. Intriguingly, the Varadero
415 population, which has substantial amounts of blue coloration on the legs and venter has a different SNP
416 than the Huallaga and Sauce morphs.

417

418 *Pteridine synthesis:*

419 Pteridines are pigments that are deposited into the xanthophores, the outermost layer of
420 chromatophores in the skin, which are thought to contribute to orange, red, yellow, and even green
421 coloration in amphibians (Duellman and Trueb 1986). Sepiapterin reductase (*spr*) is expressed primarily
422 in the xanthophores (Negishi et al. 2003) and has been shown to only be expressed in late stages of the
423 fire salamander tadpoles when yellowish color begins to appear (Sanchez et al. 2018). We found that *spr*
424 was almost exclusively expressed in the yellow-green Tarapoto morph and the yellow Huallaga morph,
425 which is a strong indication that this gene is playing a role in color pigmentation and color differences
426 between morphs in *R. imitator*. Furthermore, *spr* has been shown to be an important determinant in the
427 yellow or orange throat coloration in wall lizards (Andrade et al. 2019). In addition, we found color
428 morph specific genomic variants in the gene quinoid dihydropteridine reductase (*qdpr*), a gene which is
429 involved in the same pteridine synthesis pathway and is known to alter patterns of sepiapterin
430 production (Ponzone et al. 2004). We additionally found differences in the expression of *qdpr* over time,
431 with a fairly stark decline over development. The *qdpr* gene was also differentially expressed across
432 populations in another species of poison frog (Stuckert et al. 2019). In combination, this evidence
433 indicates that *qdpr* likely plays an important role in poison frog coloration. Similar to *qdpr,* xanthine

dehydrogenase (*xdh*) is known to influence amphibian coloration (Frost 1978; Frost and Bagnara 1979; Thorsteinsdottir and Frost 1986), exhibited a color morph specific variant in *Ranitomeya imitator,* and has been implicated in another poison frog species (Stuckert et al. 2019). *Xdh* appears to influence pterins, and as such this is another good candidate color gene for the greens, yellows, and oranges that poison frogs exhibit. We view *qdpr, spr,* and *xdh* as excellent candidates for the control of color in this system, and future work should aim to verify this.

Conclusions:

The genomics of adaptive radiations are of interest because of the strong selection imposed on phenotypes in these radiations. Further, both the specific mechanisms of color production and their genomic architecture have been poorly characterized in many groups of animals, particularly amphibians. We have produced a high-quality skin transcriptome for the polytypic poison frog *Ranitomeya imitator* which underwent a rapid mimetic radiation and used this transcriptome to characterize color gene expression patterns across color morphs and throughout development, as well as to characterize SNPs in color genes. We found fixed SNPs in *wnt3* and other genes in the Wnt signaling pathway, as well as several color genes that were differentially expressed over time which are in the same pathway. Amongst these genes, many of these are transcription factors which are important in melanocyte stem cells or melanocyte differentiation. These genes are excellent candidates for further examination via population genetics of wild frogs. We also found that pteridine genes are likely playing a role in xanthophore-related coloration. These data will provide both genomic resources for future studies of the development and the production of color and can inspire future investigations into the specific impacts that these genes have in this species and across other taxa.

Acknowledgements:

Animal use and research comply with East Carolina University's IACUC (AUP #D281). Funding for this project was provided by NSF DEB 165536 and an East Carolina University Thomas Harriot College of Arts and Sciences Advancement Council Distinguished Professorship to K Summers. We are grateful to many individuals for their help with frog husbandry in the lab, including but not limited to M Yoshioka, C Meeks, A Sorokin, K Weinfurther, R Sen, N Davison, M Johnson, M Pahl, N Aramburu. We are also grateful to Laura Bauza-Davila for her work doing RNA extractions, and Andrew Lang for guidance converting RNA to cDNA and preparing samples for sequencing.

Literature Cited:

Ai, X., A. Do, O. Lozynska, M. Kusche-gullberg, U. Lindahl, and C. P. Emerson. 2003. QSulf1 remodels the 6-O sulfation states of cell surface heparan sulfate proteoglycans to promote Wnt signaling. 162:341–351.

Andrade, P., C. Pinho, G. Pérez, D. Lanuza, S. Afonso, I. Bunikis, M. A. Carretero, N. Feiner, P. Marsik, F. Paupério, D. Salvi, and L. Soler. 2019. Regulatory changes in pterin and carotenoid genes underlie balanced color polymorphisms in the wall lizard. Proc. Natl. Acad. Sci. 1–10.

Bagnara, J. T., P. J. Fernandez, and R. Fujii. 2007. On the blue coloration of vertebrates. Pigment Cell Res. 20:14–26.

Bankevich, A., S. Nurk, D. Antipov, A. A. Gurevich, M. Dvorkin, A. S. Kulikov, V. M. Lesin, S. I. Nikolenko, S. Pham, A. D. Prjibelski, A. V. Pyshkin, A. V. Sirotkin, N. Vyahhi, G. Tesler, M. A. Alekseyev, and P. A. Pevzner. 2012. SPAdes: A new genome assembly algorithm and its applications to single-cell sequencing. J. Comput. Biol. 19:455–477.

Bolger, A. M., M. Lohse, and B. Usadel. 2014. Trimmomatic: A flexible trimmer for Illumina sequence data. Bioinformatics 30:2114–2120.

Bray, N. L., H. Pimentel, P. Melsted, and L. Pachter. 2016. Near-optimal probabilistic RNA-seq quantification. Nat. Biotechnol. 34:525–527.

Briolat, E. S., E. R. Burdfield-steel, S. C. Paul, H. R. Katja, B. M. Seymoure, T. Stankowich, and A. M. M. Stuckert. 2018. Diversity in warning coloration : selective paradox or the norm ? , doi: 10.1111/brv.12460.

Brown, J. L., V. Morales, and K. Summers. 2008. Divergence in parental care, habitat selection and larval life history between two species of Peruvian poison frogs: an experimental analysis. J. Evol. Biol.

21:1534–43.

Buchfink, B., C. Xie, and D. H. Huson. 2015. Fast and sensitive protein alignment using DIAMOND. Nat. Methods 12:59–60.

Cheung, M., and J. Briscoe. 2003. Neural crest development is regulated by the transcription factor Sox9. Development 130:5681–5693.

Coordinators, N. R. 2016. Database resources of the National Center for Biotechnology Information. Nucleic Acids Res. 44:7–19.

D'Mello, S. A. N., G. J. Finlay, B. C. Baguley, and M. E. Askarian-Amiri. 2016. Signaling pathways in melanogenesis. Int. J. Mol. Sci. 17:1–18.

Duellman, W. E., and L. Trueb. 1986. Biology of Amphibians. The John Hopkins University Press, Baltimore.

DuShane, G. P. 1935. An experimental study of the origin of pigment cells in Amphibia. J. Exp. Zool. 72:1–31.

Frost, S. K. 1978. Developmental aspects of pigmentation in the Mexican leaf frog, *Pachymedusa dacnicolor*.

Frost, S. K., and J. T. Bagnara. 1979. Allopurinol-Induced Melanism In The Tiger Salamander (Ambystoma iigrinum nebulosum). J. Exp. Zool. 209:455–465.

Gallant, J. R., V. E. Imhoff, A. Martin, W. K. Savage, N. L. Chamberlain, B. L. Pote, C. Peterson, G. E. Smith, B. Evans, R. D. Reed, M. R. Kronforst, and S. P. Mullen. 2014. Ancient homology underlies adaptive mimetic diversity across butterflies. Nat. Commun. 5:1–10. Nature Publishing Group.

Gillespie, R. 2004. Community Assembly Through Adaptive Radiation in Hawaiian Spiders. Science (80-.).

303:356–359.

Gosner, K. L. 1960. A simplified table for staging anuran embryos and larvae with notes on identification. Herpetologica 16:183–190.

Grabherr, M. G., B. J. Haas, M. Yassour, J. Z. Levin, D. A. Thompson, I. Amit, X. Adiconis, L. Fan, R. Raychowdhury, Q. Zeng, Z. Chen, E. Mauceli, N. Hacohen, A. Gnirke, N. Rhind, F. Di Palma, B. W. Birren, C. Nusbaum, K. Lindblad-Toh, N. Friedman, and A. Regev. 2011. Full-length transcriptome assembly from RNA-Seq data without a reference genome. Nat. Biotechnol. 29:644–652.

Guo, H., K. Yang, F. Deng, J. Ye, Y. Xing, Y. Li, X. Lian, and T. Yang. 2012. Wnt3a promotes melanin synthesis of mouse hair follicle melanocytes. Biochem. Biophys. Res. Commun. 420:799–804. Elsevier Inc.

Hegna, R. H., O. Nokelainen, J. R. Hegna, and J. Mappes. 2013. To quiver or to shiver: increased melanization benefits thermoregulation, but reduces warning signal efficacy in the wood tiger moth. Proc. R. Soc. B Biol. Sci. 280:20122812–20122812.

Hegna, R. H., R. A. Saporito, K. G. Gerow, and M. A. Donnelly. 2011. Contrasting colors of an aposematic poison frog do not affect predation. Ann. Zool. Fennici 48:29–38.

Hensel, J. L. J., and E. D. J. Brodie. 1976. An experimental study of aposematic coloration in the salamander *Plethodon jordani*. Copeia 59–65.

Higdon, C. W., R. D. Mitra, and S. L. Johnson. 2013. Gene expression analysis of zebrafish melanocytes, iridophores, and retinal pigmented epithelium reveals indicators of biological function and developmental origin. PLoS One 8:e67801.

Joron, M., and J. L. B. Mallet. 1998. Diversity in mimicry: Paradox or paradigm?

529 Jullien, N., A. Maudinet, B. Leloutre, J. Ringe, T. Haupl, and P. J. Marie. 2012. Downregulation of ErbB3
530 by Wnt3a Contributes to Wnt-Induced Osteoblast Differentiation in Mesenchymal Cells. J. Cell.
531 Biochem. 113:2047–2056.

532 Kannan, S., J. Hui, and K. Mazooji. 2016. Shannon: An information-optimal de novo RNA-Seq assembler.
533 1–14.

534 Kleinschmit, A., T. Koyama, K. Dejima, Y. Hayashi, K. Kamimura, and H. Nakato. 2010. Drosophila
535 heparan sulfate 6- O endosulfatase regulates Wingless morphogen gradient formation. Dev. Biol.
536 345:204–214. Elsevier Inc.

537 Korneliussen, T. S., A. Albrechtsen, and R. Nielsen. 2014. ANGSD: Analysis of Next Generation
538 Sequencing Data. BMC Bioinformatics 15:1–13.

539 Kronforst, M. R., D. D. Kapan, and L. E. Gilbert. 2006. Parallel genetic architecture of parallel adaptive
540 radiations in mimetic Heliconius butterflies. Genetics 174:535–539.

541 Kronforst, M. R., and R. Papa. 2015. The functional basis of wing patterning in *Heliconius* butterflies: The
542 molecules behind mimicry. Genetics 200:1–19.

543 Kunte, K., W. Zhang, A. Tenger-Trolander, D. H. Palmer, A. Martin, R. D. Reed, S. P. Mullen, and M. R.
544 Kronforst. 2014. doublesex is a mimicry supergene. Nature 507:229–232.

545 Larue, L., and V. Delmas. 2006. The WNT/Beta-catenin pathway in melanoma. Front. Biosci. 11:733–742.

546 Li, B., X. long He, Y. ping Zhao, Q. nan Zhao, Unierhu, D. yi Bai, and D. Manglai. 2014. Tyrosinase-related
547 protein 1 (TYRP1) gene polymorphism and skin differential expression related to coat color in
548 Mongolian horse. Livest. Sci. 167:58–64. Elsevier.

549 Lister, J., C. Robertson, T. Lepage, S. Johnson, and D. Raible. 1999. Nacre Encodes a Zebrafish

550 Microphthalmia-Related Protein That Regulates Neural-Crest-Derived Pigment Cell Fate.
551 Development 126:3757–3767.

552 MacManes, M. D. 2014. On the optimal trimming of high-throughput mRNA sequence data. Front.
553 Genet. 5:1–7.

554 MacManes, M. D. 2017. The Oyster River Protocol: A multi assembler and kmer approach for de novo
555 transcriptome assembly. Doi.Org 177253.

556 Mallet, J., and N. H. Barton. 1989. Strong natural selection in a warning-color hybrid zone. Evolution (N.
557 Y). 43:421–431.

558 Marek, P. E., and J. E. Bond. 2009. A Müllerian mimicry ring in Appalachian millipedes. Proc. Natl. Acad.
559 Sci. U. S. A. 106:9755–60.

560 Martin, A., R. Papa, N. J. Nadeau, R. I. Hill, B. A. Counterman, G. Halder, C. D. Jiggins, M. R. Kronforst, A.
561 D. Long, W. O. McMillan, and R. D. Reed. 2012. Diversification of complex butterfly wing patterns
562 by repeated regulatory evolution of a Wnt ligand. Proc. Natl. Acad. Sci. 109:12632–12637.

563 Martin, A., and R. D. Reed. 2014. Wnt signaling underlies evolution and development of the butterfly
564 wing pattern symmetry systems. Dev. Biol. 395:367–378. Elsevier.

565 Mi, H., X. Huang, A. Muruganujan, H. Tang, C. Mills, D. Kang, and P. D. Thomas. 2017. PANTHER version
566 11: Expanded annotation data from Gene Ontology and Reactome pathways, and data analysis tool
567 enhancements. Nucleic Acids Res. 45:D183–D189.

568 Negishi, S., K. Fujimoto, and S. Katoh. 2003. Localization of sepiapterin reductase in pigment cells of
569 Oryzias latipes. Pigment Cell Res. 16:501–503.

570 Ng, A., R. A. Uribe, L. Yieh, R. Nuckels, and J. M. Gross. 2009. Zebrafish mutations in gart and paics

identify crucial roles for de novo purine synthesis in vertebrate pigmentation and ocular development. Development 136:2601–2611.

Nishikawa, H., T. Iijima, R. Kajitani, J. Yamaguchi, T. Ando, Y. Suzuki, S. Sugano, A. Fujiyama, S. Kosugi, H. Hirakawa, S. Tabata, K. Ozaki, H. Morimoto, K. Ihara, M. Obara, H. Hori, T. Itoh, and H. Fujiwara. 2015. A genetic mechanism for female-limited Batesian mimicry in *Papilio* butterfly. Nat. Genet. 47:405–409. Nature Publishing Group.

Nokelainen, O., R. H. Hegna, J. H. Reudler, C. Lindstedt, and J. Mappes. 2012. Trade-off between warning signal efficacy and mating success in the wood tiger moth. Proc. Biol. Sci. 279:257–65.

Nosil, P., and B. J. Crespi. 2006. Experimental evidence that predation promotes divergence in adaptive radiation. Proc. Natl. Acad. Sci. 103:9090–9095.

Paluh, D. J., M. M. Hantak, and R. A. Saporito. 2014. A test of aposematism in the dendrobatid poison frog *Oophaga pumilio*: The importance of movement in clay model experiments. J. Herpetol. 48:249–254.

Park, H. Y., M. Kosmadaki, M. Yaar, and B. A. Gilchrest. 2009. Cellular mechanisms regulating human melanogenesis. Cell. Mol. Life Sci. 66:1493–1506.

Pimentel, H., N. L. Bray, S. Puente, P. Melsted, and L. Pachter. 2017. Differential analysis of RNA-seq incorporating quantification uncertainty. Nat. Methods 14:687–690.

Ponzone, A., M. Spada, S. Ferraris, I. Dianzani, and L. De Sanctis. 2004. Dihydropteridine reductase deficiency in man: From biology to treatment. Med. Res. Rev. 24:127–150.

Reed, R. D., R. Papa, A. Martin, H. M. Hines, M. R. Kronforst, R. Chen, G. Halder, H. F. Nijhout, and W. O. Mcmillan. 2011. optix drives the repeated convergent evolution of butterfly wing pattern mimicry. Science (80-.). 333:1137–1141.

593 Rieder, S., S. Taourit, D. Mariat, and B. Langlois. 2001. Mutations in the agouti (ASIP), the extension (
594 MC1R), and the brown (TYRP1) loci and their association to coat color phenotypes in horses (
595 Equus caballus). 455:450–455.

596 Rudh, A., and A. Qvarnström. 2013. Adaptive colouration in amphibians. Semin. Cell Dev. Biol. 24:553–
597 561. Elsevier Ltd.

598 Ruxton, G. D., T. N. Sherratt, and M. P. Speed. 2004. Avoiding attack: The evolutionary ecology of
599 crypsis, warning signals and mimicry.

600 Saenko, S. V., J. Teyssier, D. van der Marel, and M. C. Milinkovitch. 2013. Precise colocalization of
601 interacting structural and pigmentary elements generates extensive color pattern variation in
602 *Phelsuma* lizards. BMC Biol. 11:105.

603 Sanchez, E., E. Küpfer, D. J. Goedbloed, A. W. Nolte, T. Lüddecke, S. Schulz, M. Vences, and S. Steinfartz.
604 2018. Morphological and transcriptomic analyses reveal three discrete primary stages of
605 postembryonic development in the common fire salamander, *Salamandra salamandra*. J. Exp.
606 Zool. Part B Mol. Dev. Evol. 330:96–108.

607 Schluter, D. 1995. Adaptive radiation in sticklebacks: Trade-offs in feeding performance and growth.
608 Ecology 76:82–90.

609 Seehausen, O. 2006. African cichlid fish: a model system in adaptive radiation research. Proc. Biol. Sci.
610 273:1987–1998.

611 Sherratt, T. N. 2006. Spatial mosaic formation through frequency-dependent selection in M??llerian
612 mimicry complexes. J. Theor. Biol. 240:165–174.

613 Simão, F. A., R. M. Waterhouse, P. Ioannidis, E. V. Kriventseva, and E. M. Zdobnov. 2015. BUSCO:
614 Assessing genome assembly and annotation completeness with single-copy orthologs.

615 Bioinformatics 31:3210–3212.

616 Sköld, H. N., S. Aspengren, K. L. Cheney, and M. Wallin. 2016. Fish Chromatophores-From Molecular
617 Motors to Animal Behavior. Int. Rev. Cell Mol. Biol. 321:171–219. Elsevier Inc.

618 Smith-Unna, R., C. Boursnell, R. Patro, J. M. Hibberd, and S. Kelly. 2016. TransRate: Reference-free
619 quality assessment of de novo transcriptome assemblies. Genome Res. 26:1134–1144.

620 Song, X., C. Xu, Z. Liu, Z. Yue, L. Liu, T. Yang, B. Cong, and F. Yang. 2017. Comparative transcriptome
621 analysis of mink (*Neovison vison*) skin reveals the key genes involved in the melanogenesis of black
622 and white coat colour. Sci. Rep. 7:1–11. Springer US.

623 Stuckert, A. M. M., E. Moore, K. P. Coyle, I. Davison, M. D. MacManes, R. Roberts, and K. Summers.
624 2019. Variation in pigmentation gene expression is associated with distinct aposematic color
625 morphs in the poison frog, Dendrobates auratus. BMC Evol. Biol. 19:1–15.

626 Stuckert, A. M. M., R. A. Saporito, P. J. Venegas, and K. Summers. 2014a. Alkaloid defenses of co-mimics
627 in a putative Müllerian mimetic radiation. BMC Evol. Biol. 14:1–8.

628 Stuckert, A. M. M., P. J. Venegas, and K. Summers. 2014b. Experimental evidence for predator learning
629 and Müllerian mimicry in Peruvian poison frogs (*Ranitomeya*, Dendrobatidae). Evol. Ecol. 28:413–
630 426.

631 Supple, M. a, H. M. Hines, K. K. Dasmahapatra, J. J. Lewis, D. M. Nielsen, C. Lavoie, D. a Ray, C. Salazar,
632 W. O. Mcmillan, and B. a Counterman. 2013. Genomic architecture of adaptive color pattern
633 divergence and convergence in *Heliconius* butterflies. Genome Res. 23:1248–1257.

634 Symula, R., R. Schulte, and K. Summers. 2001. Molecular phylogenetic evidence for a mimetic radiation
635 in Peruvian poison frogs supports a Müllerian mimicry hypothesis. Proc. R. Soc. B Biol. Sci.
636 268:2415–21.

637 Symula, R., R. Schulte, and K. Summers. 2003. Molecular systematics and phylogeography of Amazonian
638 poison frogs of the genus *Dendrobates*. Mol. Phylogenet. Evol. 26:452–475.

639 Takeda, K., K. I. Yasumoto, R. Takada, S. Takada, K. I. Watanabe, T. Udono, H. Saito, K. Takahashi, and S.
640 Shibahara. 2000. Induction of melanocyte-specific microphthalmia-associated transcription factor
641 by Wnt-3a. J. Biol. Chem. 275:14013–14016.

642 Team, R. C. 2017. R Development Core Team.

643 Thorsteinsdottir, S., and S. K. Frost. 1986. Pigment cell differentiation: The relationship between pterin
644 content, allopurinol treatment, and the melanoid gene in axolotls. Cell Differ. 19:161–172.

645 Vestergaard, J. S., E. Twomey, R. Larsen, K. Summers, and R. Nielsen. 2015. Number of genes controlling
646 a quantitative trait in a hybrid zone of the aposematic frog Ranitomeya imitator. Proc. R. Soc. B
647 282:20141950.

648 Videira, I. F. D. S., D. F. L. Moura, and S. Magina. 2013. Mechanisms regulating melanogenesis. An. Bras.
649 Dermatol. 88:76–83.

650 Wilson, J. S., J. P. Jahner, M. L. Forister, E. S. Sheehan, K. A. Williams, and J. P. Pitts. 2015. North
651 American velvet ants form one of the world's largest known Müllerian mimicry complexes. Curr.
652 Biol. 25:R704–R706. Elsevier.

653 Wolnicka-Glubisz, A., A. Pecio, D. Podkowa, L. M. Kolodziejczyk, and P. M. Plonka. 2012. Pheomelanin in
654 the skin of *Hymenochirus boettgeri* (Amphibia: Anura: Pipidae). Exp. Dermatol. 21:537–540.

655 Xu, Y., X. H. Zhang, and Y. Z. Pang. 2013. Association of tyrosinase (TYR) and tyrosinase-related protein 1
656 (TYRP1) with melanic plumage color in Korean quails (Coturnix coturnix). Asian-Australasian J.
657 Anim. Sci. 26:1518–1522.

658 Ziegler, I. 2003. The pteridine pathway in zebrafish: Regulation and specification during the

659 determination of neural crest cell-fate. Pigment Cell Res. 16:172–182.

660